

RSC Advances



This is an *Accepted Manuscript*, which has been through the Royal Society of Chemistry peer review process and has been accepted for publication.

Accepted Manuscripts are published online shortly after acceptance, before technical editing, formatting and proof reading. Using this free service, authors can make their results available to the community, in citable form, before we publish the edited article. This *Accepted Manuscript* will be replaced by the edited, formatted and paginated article as soon as this is available.

You can find more information about *Accepted Manuscripts* in the [Information for Authors](#).

Please note that technical editing may introduce minor changes to the text and/or graphics, which may alter content. The journal's standard [Terms & Conditions](#) and the [Ethical guidelines](#) still apply. In no event shall the Royal Society of Chemistry be held responsible for any errors or omissions in this *Accepted Manuscript* or any consequences arising from the use of any information it contains.

Pt atoms Stabilized on Hexagonal Boron Nitride as Efficient Single-Atom Catalysts for CO Oxidation: A First-principles Investigation

Xin Liu^{†,*}, *Ting Duan*[†], *Changgong Meng*[†], *Yu Han*[‡]

[†] School of Chemistry, Dalian University of Technology, Dalian, 116024, P. R. China

[‡] Advanced Membranes and Porous Materials Center, King Abdullah University of Science and Technology, Thuwal, 23955-6900, Kingdom of Saudi Arabia

*Corresponding Author:

Dr. Xin Liu

Tel: +86-411-84986343

Email: xliu@dlut.edu.cn

ABSTRACT

Taking the CO oxidation as a probe, we investigated the electronic structure and reactivity of Pt atoms stabilized by vacancy defects on hexagonal boron nitride (h-BN) by first-principles-based calculations. As a joint effect of the high reactivity of both a single Pt atom and a boron vacancy defect (PtBV), the Pt-N interaction is -4.40 eV and is already strong enough to prohibit the diffusion and aggregation of the stabilized Pt atom. Facilitated by the upshifted Pt-d states originated from the Pt-N interaction, the barriers for CO oxidation through the Langmuir–Hinshelwood mechanism for formation and dissociation of peroxide-like intermediate and the regeneration are as low as 0.38, 0.10 and 0.04 eV, respectively, suggesting the superiority of PtBV as a catalyst for low temperature CO oxidation.

KEYWORDS: hexagonal boron nitride; vacancy; defects; Pt; CO; oxidation;

1. INTRODUCTION

The catalytic oxidation of carbon monoxide (CO) has attracted extensive attentions for several decades, not only for its important role in emission control of environmental-harmful pollutants, including CO, from combustion, industrial chemical processes and etc, but also for its simple stoichiometry as well as industrial significance, as a prototype catalytic reaction in surface chemistry that plays an essential role in evaluating activity, selectivity and durability of a catalyst. Deposited nanoparticles (NPs) of transition metals (TMs), including Pt¹⁻³, Pd,^{4, 5} Rh^{6, 7}, Au^{8, 9} and etc, can catalyze CO oxidation, but these TMs are expensive and their affinity to CO are stronger than that to O₂. As a result, high operating temperature is always required to keep them efficient.¹⁰ Scientists have been working continuously to develop efficient catalysts for low temperature CO oxidation.¹¹⁻¹³

As the reactivity of a TM atom is determined by the energy levels of TM-d states that are sensitive to the local coordination environments, unsaturated TM atoms at edge and corner of NPs are the reaction sites and the catalytic performance depends more strongly on the morphology than the size of TM NPs.¹⁴⁻¹⁷ In this sense, downsizing the size of NPs to sub-nano scale or even single atom to achieve a high density of active sites while keeping or even promoting the catalytic performance is highly desired and will lead to a highly efficient usage of the precious TMs.¹⁸ As the size of NPs goes down, the profits of the TM-support interaction to the catalytic performance can be multifold in principle, which not only alters the spacial and energetic distribution of TM states that are essential for activation of the adsorbates,¹⁹⁻²³ but also strongly impacts the free energy of the assembly of TM atoms that set the durability, the atomic stacking and the morphology of the TM NPs.²⁴⁻²⁷ In this sense, a careful screening of the metal-support interactions would be vital to rationalize the design of mono-dispersed ultrafine TM NPs

or single TM atoms as efficient catalyst for a specific reaction. Combining the highly active monodispersed TM atoms and suitable support materials, several single-atom catalysts have been found efficient for CO oxidation, such as Pt/FeO_x,¹² Pt/Al₂O₃,²⁸ Au/FeO_x,²⁹ Pd/CeO₂,³⁰ Ir/Fe(OH)_x,¹³ Ag/MnO_x,³¹ Pt/Graphene^{32, 33} and etc. More recently, Au, Cu, Fe, Pt atoms embedded graphene have also been predicted to be highly effective for CO catalytic oxidation theoretically.³³⁻³⁷

Hexagonal boron nitride (*h*-BN), which has similar planar structure like graphene but with different chemical and physical properties, has drawn considerable attention in recent years.³⁸⁻⁴¹ Due to the different electronegativity of B and N, *h*-BN is more ionic, leading the interaction and charge transfer with deposited TM atoms to be different from those on graphene. There are various defects, such as vacancies and boundaries, exist in the as synthesized *h*-BN sheets and are ready to anchor TM NPs. These defects could be created by controlled electron beam irradiation due to the knock-on effect of the incident electrons.⁴² As the threshold beam energy for knock-on of B is smaller than that of N, B vacancies (BVs) can be formed more easily during electron beam bombardment. Therefore, all the edge-terminating atoms around the vacancies must be N.^{43, 44} The existence of these defects over *h*-BN provides a new platform for fabrication of finely dispersed TM NPs or single-atom catalysts.⁴⁵ Though Cu, Co, Ru, Fe and Au atoms embedded in *h*-BN were proposed to be effective for CO oxidation, the important role of interfacial interaction hasn't been explained in detail.⁴⁵⁻⁴⁹

Inspired by previous works and to rational the design of single-atom catalysts, we investigated the electronic structure and predicted the catalytic performance in CO oxidation of Pt atoms stabilized by BV on *h*-BN by first-principles-based calculations. We showed that, due to the interfacial Pt-N interaction, not only the Pt atoms are effectively stabilized from further diffusion

and aggregation, but also some Pt-d states are upshifted to the E_F so that PtBV exhibits unexpected reactivity. Facilitated by these upshifted Pt-d states that eventually satisfy the requirements for O_2 activation and subsequent reactions among coadsorbates, the CO oxidation over PtBV prefers to proceed through the Langmuir–Hinshelwood mechanism and the calculated barriers are among the lowest values ever reported, suggesting the superiority of PtBV as catalyst for low temperature CO oxidation. The rest of the paper is organized as the following: the theoretical methods and computational details are described in Section 2, the results are presented and discussed in Section 3 and concluded in Section 4.

2. THEORETICAL METHODS

The first-principles-based calculations were carried out using Perdew-Burke-Ernzerhof functional within the formulation of general gradient approximation in combination with DFT semicore pseudopotentials as implemented in the DMol³ package.⁵⁰⁻⁵³ A hexagonal 5×5 supercell of h-BN was used to mimic the h-BN support and the Pt/h-BN composites, it contains only a single layer of h-BN. The thickness of the supercell was set to be larger than 20 Å to avoid interaction among neighboring images. The structures of h-BN support and the Pt/h-BN composites were firstly relaxed with empirical potentials^{54,55} and were then fully relaxed within the ab-initio scheme until the residue forces were smaller than 1×10^{-2} eV/Å. The transition states (TSs) were located through the synchronous method with conjugated gradient refinements and verified with frequency analysis.⁵⁶ All the calculations were performed with a real-space global orbital cutoff radius of 4.6 Å and a convergence criterion of 2×10^{-4} eV on the total energy. A Γ -centered $4 \times 4 \times 1$ Monkhorst-Pack k -point grid was used for structural relaxation and TSs location, while a $20 \times 20 \times 1$ grid was used for electronic structure analysis.⁵⁷ The amount of charge transfer was evaluated within the Hirshfeld scheme.⁵⁸ With the above setup,

the bulk lattice parameter of face-center-cubic Pt and h-BN was reproduced as 3.98 and 2.52 Å, respectively.^{59,60} Test calculations with a 9×9 h-BN supercell gave essentially the same results.

The binding energy (E_b) of Pt atom onto h-BN was calculated as the energy difference between the Pt/h-BN composites and the clean h-BN plus a freestanding Pt atom, following Eqn (1).

$$E_b = E_{PtBN} - (E_{Pt} + E_{BN}) \quad (1)$$

The adsorption energies (E_{ad}) of CO, O₂, O and CO₂ were calculated as the energy difference between the absorbed PtBN and the gas adsorbate plus the bare PtBN, following Eqn (2).

$$E_{ad} = E_{adsorbate+PtBN} - (E_{PtBN} + E_{adsorbate}) \quad (2)$$

3. RESULTS AND DISCUSSIONS

We first investigated the deposition of monodispersed Pt atoms onto pristine h-BN (PBN) and found Pt atoms bind weakly with PBN. The E_b s for Pt deposition on top of a N atom (AtopN), a B atom (AtopB) and on top of the center of a 3B3N ring (Hol) are -0.67, -0.70 and -0.67 eV, respectively. We also considered the Pt atomic deposition in the middle of adjacent B and N atoms, but the Pt atom will diffuse to AtopB during structure relaxation. In the most plausible deposition structure, the Pt atom stands above a B atom and there is a charge transfer of 0.11 |e| to the surface. Stabilization of single TM atoms whose surface free energy is extremely large under realistic reaction condition is one of the key problems in fabrication of practical single atom catalysts.^{26,27} The small differences among the E_b at various deposition sites (0.03 eV), the low atomic diffusion barrier (0.03 eV) and the small charge transfer (0.11 |e|) suggest that PBN cannot stabilize monodispersed Pt atoms. To minimize the surface free energy, Pt atoms will diffuse to form large NPs as the amount of Pt deposition increases. This problem can be partially solved if there are defects on the support surface that can form mature interaction with the TM atoms and effectively stabilize them.⁶¹⁻⁶³ Recent investigation on structure of h-BN shows that

there are many defects, including vacancies, exist after electron-beam bombardment.⁴² As the threshold energy for B is smaller than that N atoms, formation of BV would be much easier and the defect edges should be terminated by N atoms.⁴³ Therefore, BV was considered as the typical defects over *h*-BN.

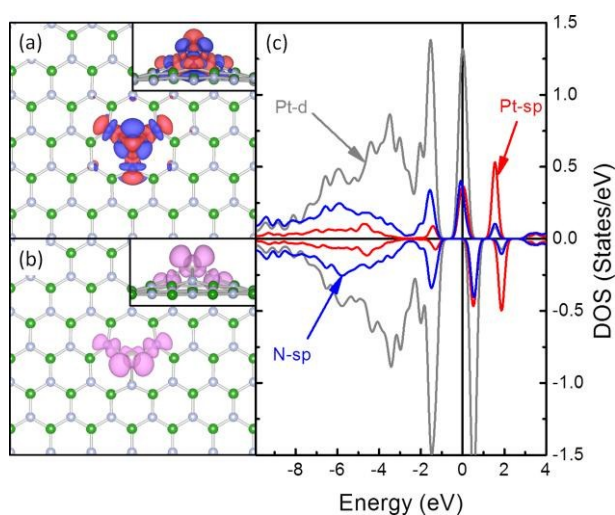


Figure 1. Structure and contour plots of differential charge density (a) and charge density of selected state (b) and DOS of PtBV (c). (B: Green; C: Brown; N: Light blue; Pt: Silver. The contour value of the charge density is ± 0.005 a.u. The charge accumulation regions are in red while the charge depletion regions are in blue.)

Due to the larger size of Pt atoms as compared with B atoms, when a Pt atom is placed above a BV, it is 1.52 \AA above the basal plane of *h*-BN after geometry optimization. Compared with the case of Pt atomic deposition on PBN, the charge on Pt atom at the BV (PtBV) is enhanced to $0.45 |e|$. The differential charge density shows that there are significant charge accumulation regions between the Pt atoms and the N atoms, suggesting the formed interactions are partially covalent (Figure 1). The E_b at BV (-4.40 eV) is thus enhanced by more than five folds as compared with that on PBN (-0.70 eV).⁴⁵ The enhanced E_b of PtBV also makes the outward

diffusion of Pt atom to its neighboring Hol site endothermic by 3.70 eV. The computed diffusion barrier is 4.59 eV and is much higher than the Pt atomic diffusion barrier of 0.03 eV on PBN, so the outward diffusion of BV stabilized Pt atoms is kinetically prohibited.

The projected density of states (PDOS) of Pt-sp, Pt-d and N-sp states of Pt and N atoms at BV are plotted to highlight the origin of the enhanced E_b in PtBV (Figure 1). The DOS of BV is characterized with sharp peaks inside the bulk band gap of h-BN.⁴⁹ After Pt deposition, the peaks at the E_F and the sharp spikes inside the band gap corresponding to N-sp states are shifted downwards and overlap with the Pt-sp and Pt-d states, showing the strong hybridization among these states. This, together with the differential charge density, suggests that the stabilized Pt atom uses its valence states to interact with the defective states of the BV. The electron density of the hybridized state at the E_F was extracted in Figure 1, which is localized on the PtBV and is mainly contributed by the interaction between the in-plane components of Pt-d states and the N-sp states of N atoms around the vacancy. This confirms that, some of the dangling Pt-d states are upshifted to E_F and resonance with N-sp states due to the Pt-N interaction. We compared the DOS of PtBV and Pt(111) in Figure S1 and found that the workfunction of PtBV is 1.26 eV smaller than that of Pt(111). The energy levels of localized d states of transition metals are known to be vital for the activation of adsorbed reactants and subsequent reactions, while the workfunction determines the easiness to donate electrons from frontier states. The dominant contribution of Pt-d states at E_F and the decreased workfunction suggest that the transfer of electrons in Pt-d states to adsorbates from PtBV would be much easier than from surface atoms on Pt(111). In this sense, PtBV may exhibit higher reactivity in activation of adsorbed CO and O₂ for CO oxidation.

Table 1. The E_{ad} s and the most plausible structures of various reaction species adsorption on PtBV.

Species	E_{ad}^a (eV)	Bonding Details	
		Bond	Length (Å)
CO	-1.92	C-O	1.16
		Pt-C	1.91
O ₂	-1.87 ^b	O-O	1.37
		Pt-O	2.11
		Pt-O	2.11
O	-3.94 ^b	Pt-O	1.82
CO ₂	-0.08	Pt-O	2.24
		C-O	1.20
		C-O	1.26

^a. The E_{ad} is calculated as the energy difference between the species adsorbed on PtBV and the gaseous species plus the bare PtBV according to eqn 2. ^b. Due to the unpaired d-electron on Pt, the ground state of PtBV is doublet. The adsorption of O₂ and O in quartet was also considered, but was found less plausible by 0.91 and 1.02 eV, respectively, as compared with those in doublet.

We then investigated the adsorption of reaction species to deduce the thermodynamics of the reaction (Table 1 and Figure 2). For CO oxidation over PtBV, the possible reaction species are O₂, CO, O and CO₂. As h-BN is chemically inert, O₂, CO and CO₂ are only physisorbed on PBN. In accordance with the upshift of Pt-d states, the calculated E_{ad} for CO on PtBV is -1.92 eV and is stronger than that over compact Pt surfaces.⁵⁹ In this configuration, the CO lies in the reverse direction of one of the Pt-N bonds and the Pt-C distance is 1.91 Å, suggesting a typical chemical bond is formed. The E_{ad} of O₂ is -1.87 eV, corresponding to O₂ lying parallel to the h-BN surface immediately on top of Pt atom with the Pt-O distances are both 2.11 Å. Both CO and O₂ interact strongly with PtBV, indicating that both of them can be readily adsorbed onto the PtBV at moderate temperatures. As for O atom, it prefers to stand 1.82 Å on top of the Pt atom with the

Pt-O direction vertical to the h-BN support and the corresponding E_{ad} is -3.94 eV. The enhancement of O E_{ad} can be understood as the result of removing of repulsive interaction among negative charge absorbed O atoms as compared with the case of O_2 . This phenomenon is widely observed in coverage dependent O adsorption on surfaces of transition metals and alloys.^{64, 65} We also considered the dissociation adsorption of O_2 , but found that the adsorption of 2 O atoms is less plausible as compared with that of O_2 by 0.38 eV and the barrier for O_2 dissociation is 0.92 eV. As the coadsorbed O or CO will further enlarge this barrier, the dissociative adsorption of O_2 less likely to take place. The E_{ad} of CO_2 is enhanced moderately to -0.17 eV over PtBV. Due to the interaction with the Pt atom, the nearest Pt-C and Pt-O distances are 2.17 and 2.24 Å, respectively, and the $\angle\text{O-C-O}$ angle is distorted to 145.6° as compared with 180° before adsorption.

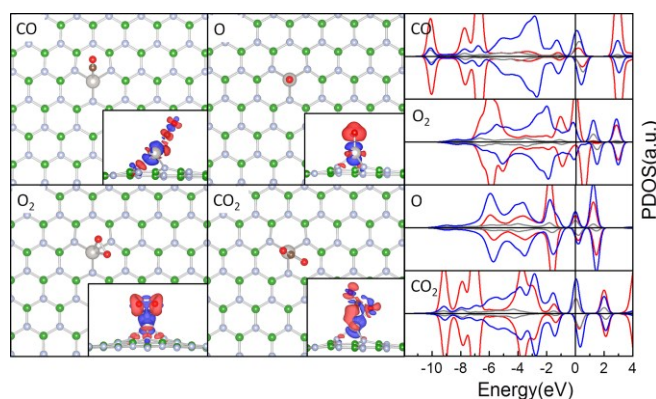


Figure 2. The most plausible adsorption structures and contour plots of differential charge density (left panel), and the corresponding DOS curves (right panel) for CO, O_2 , O and CO_2 adsorption on PtBV. (C: Brown; Pt: Silver; N: Light blue; B: Green; O: Red. For the contour plots, the charge accumulation regions are rendered in red while the charge deplete regions are shown in blue. The contour value of the differential charge density is ± 0.005 a.u. The DOS curves of adsorbed species are in red, those of Pt-sp and Pt-d are in blue and grey, respectively.

The DOS curves are aligned by the calculated energy levels of highest occupied states of free species.)

The DOS curves of adsorbates and the contour plots of differential charge density were analyzed to understand mechanism of enhanced adsorption. Due to the formation of Pt-C and Pt-O bonds, the shape and distribution of DOS peaks corresponding to frontier states of CO, O₂ and CO₂ change significantly. The CO and O₂ 5σ states are shifted to lower energy, their 2π states and the π antibonding states of CO₂ are split into parts and partially downshifted to below the E_F to resonance strongly the Pt-d and Pt-sp states, showing the hybridization and charge transfer among them. Accordingly, there are large charge depletion regions between C-O, O-O and O=C-O indicating that there are charge transfer to the 2π states of CO and O₂ and the π antibonding states of CO₂, and these adsorbates are thus activated. This is further supported by the elongation of the C-O distances in CO and CO₂ and the O-O distance in O₂ after adsorption to 1.16, 1.26 and 1.37 Å, respectively. The DOS curve of O-sp for O adsorption is similar to that of O₂, suggesting the effectiveness of PtBV for O₂ activation. The amounts of charge transfer to CO, O₂, O and CO₂ after adsorption are 0.06, 0.29, 0.32 and 0.25 |e|, respectively. As the charge transfer is always to the adsorbents, there are charge depletion regions on the Pt atom. Charge accumulation regions can be observed between Pt-C, Pt-O for CO, O₂ and CO₂ adsorption, indicating that the newly formed Pt-C and Pt-O bonds are partially covalent.

We noticed that in the most plausible adsorption configurations of CO and O₂, the Pt atom is not fully coordinated in a distorted octahedral. This implies that bi-molecular adsorption may take place over PtBV. As the adsorption of CO is preferred by 0.05 eV over O₂, the coadsorption of 2 O₂ is not stable in existence of trace amount of CO. The coadsorption of 2 CO and one CO with one O₂ were investigated. The coadsorption of one CO and one O₂ is an exothermic process

and the corresponding E_{ad} is -3.04 eV, which not only overwhelms the coadsorption 2 CO (-2.92 eV), but is also stronger than the individual adsorption of either CO and O₂. In this sense, there is no CO poisoning problem over PtBV and the CO oxidation may initiate with the coadsorption of CO and O₂ on the same Pt atom stabilized by BV.

In general, CO oxidation can take place through 2 mechanisms, namely the Langmuir-Hinshelwood (LH) and the Eley-Rideal (ER) mechanism, depending on the detailed nature of the catalyst.⁶⁶ The ER mechanism initiates with the direct reaction of one gaseous reactant (such as CO) with the another activated reactant at the reaction center (such as adsorbed O atom and activated O₂). In the typical CO oxidation initiated with reaction between gaseous CO and activated O₂, the formation or dissociation of CO₃-like intermediate may set the overall reaction rate, because the gaseous CO is not activated for the formation of the CO₃-like intermediate, which is always too stable for subsequent reactions. Different from the ER mechanism, the CO oxidation following LH mechanism starts with the interaction between the coadsorbed CO and O₂ molecules for formation of a peroxide-like O-C-O-O intermediate. As the coadsorbed CO and O₂ are partially negatively charged and repulsive to each other, the formation of the peroxide becomes demanding and sets the rate of the whole process. Because the coadsorption of CO and O₂ is preferred over PtBV and satisfies the requirements for initiation of CO oxidation through LH mechanism, which is also the CO oxidation mechanism over Au, Cu and Pt atoms embedded in graphene and h-BN and on Au clusters deposited over MgO and TiO₂, we focused on CO oxidation over PtBV with reaction between coadsorbed CO and O₂.^{8, 33-35, 49, 67} The most plausible adsorption structure of CO and O₂, together with the atomic structures at various states along the minimum-energy path (MEP) following the LH mechanism are shown in Figure 3, with the corresponding structural parameters listed in Table 2.

Table 2. Structural Parameters for Various States along the MEP for the CO Oxidation over PtBV through LH Mechanism.

States	d_{C-O}^a (Å)	d_{C-Pt}^a (Å)	d_{C-O1}^a (Å)	d_{C-O2}^a (Å)	d_{O1-O2}^a (Å)	d_{O1-Pt}^a (Å)	d_{O2-Pt}^a (Å)	\angle_{O-C-O1}^b (°)	\angle_{O-C-O2}^b (°)
LH-IS1	1.16	1.95	3.08	--	1.29	2.14	--	113.2	--
LH-TS1	1.17	2.02	1.96	--	1.35	2.10	--	113.7	--
LH-MS1	1.21	2.06	1.39	--	1.48	2.07	--	120.8	--
LH-TS2	1.22	2.11	1.32	--	1.75	1.99	--	123.8	--
LH-FS1	1.18	4.23	1.18	--	3.23	1.82	--	178.1	--
LH-IS2	1.14	3.97	--	3.10	--	--	1.82	--	95.7
LH-TS3	1.14	3.01	--	2.86	--	--	1.84	--	102.5
LH-FS2	1.20	2.17	--	1.26	--	--	2.24	--	145.6

^a The distance between specific atoms. Please see Figure 3 and the context for the nomination of atoms.

^b The angle among O-C-O. This angle is 120° in CO₃²⁻ and is 180° in free CO₂.

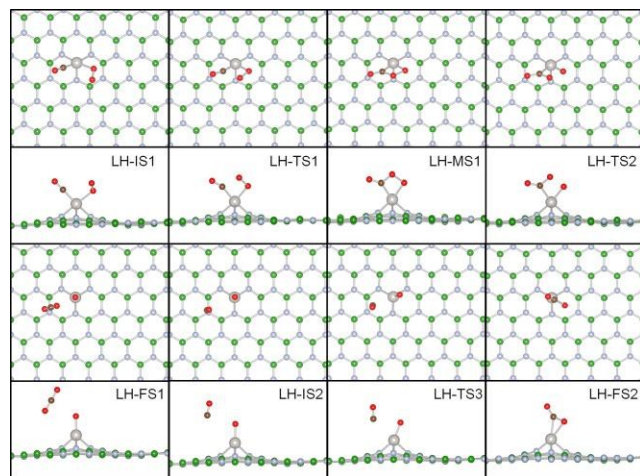


Figure 3. Top views (Top panel) and side views (Bottom panel) of local configurations of the adsorbates on the PtBV at various states along the MEP via the LH mechanism, including the initial states (LH-IS1 and LH-IS2), transition states (LH-TS1, LH-TS2 and LH-TS3), intermediate states (LH-MS1 and LH-FS1) and the final state (LH-FS2). (C: Brown; N: Light Blue; B: Green; O: Red; Pt: Silver.)

Though CO and O₂ gain electrons from PtBV in the coadsorbed configuration (LH-IS1), the Hirshfeld charge on the C atom of CO is +0.10|e| while that on O1 atom of O₂ is -0.10 |e|. This drives the O1 of O₂ to move toward C atom of CO to reach the transition state (LH-TS1) that connects LH-IS1 to LH-MS1 on the MEP. During this endothermic process, both the structures of CO and O₂ are distorted for formation of C-O1 interaction. The O1-O2 distance in O₂ is stretched from 1.29 Å in LH-IS1 to 1.35 Å in LH-TS1, while the C-O distance is elongated from 1.16 Å after adsorption to 1.17 Å. As a result, the C-O1 distance decreases from 3.08 Å in LH-IS1 to 1.96 Å in LH-TS1. The energy barrier for the formation of LH-MS1 is 0.38 eV and a peroxide-like O2-O1-C-O complex is thus formed. Because the C-O1 interaction is mature in LH-MS1, the O1-O2 distance is further elongated to 1.48 Å. The O-O distance of this length scale has been only be observed in peroxide, showing the instability of LH-MS1 and the easiness for scission of the O-O bond to take place. The formation of LH-MS1 is exothermic by 0.45 eV as compared with LH-TS1 and the localized charge is balanced with the formation of C-O1 bond,. As a consequence of the instable peroxide bond, LH-MS1 dissociates by breaking the O1-O2 bond and forms a physisorbed CO₂ and an O atom adsorbed on PtBV (LH-FS1). Driven by the strong exothermic formation of the C=O bond, the barrier for the formation of physisorbed CO₂ from LH-MS1 is only 0.10 eV. The tendency to strengthen the C-O1 interaction and weaken the O1-O2 and Pt-C interaction is apparent at the transition state (LH-TS2), where the O1-O2 distance is already as long as 1.75 Å, the Pt-C distance has reached 2.11 Å, while the C-O1 distance is shortened from 1.39 Å to 1.32 Å. This suggests that the dissociation of LH-MS1 is a spontaneous process and is ready to take place at low temperatures. As the E_{ad} of CO₂ is only at the level of -0.10 eV, the desorption of CO₂ in LH-FS1 can also be considered barrierless.

The subsequent reaction takes place between a gaseous CO molecule and the adsorbed O atom over PtBV for the regeneration of Pt atom as available reaction center. A configuration of the CO molecule stands more than 3.0 Å away from the adsorbed atomic O on PtBV was selected as the initial state (LH-IS2). The final state was set to the configuration that CO₂ adsorbed on PtBV (LH-FS2). While the gaseous CO approaches to PtBV, the C atom of CO gets partially positively charged and interacts electrostatically with the remnant O atom to reach LH-TS3. Within LH-TS3, the Pt-C distance is decreased from 3.97 Å in LH-IS2 to 3.01 Å and the C-O2 distance is also decreased from 3.10 to 2.86 Å, showing that due to the formation of interaction between CO and O atom, the CO molecule is pushed to the PtBV in this endothermic process. Because of the high reactivity of the adsorbed O atom and the strong exothermic formation of CO₂, the reaction barrier for formation of LH-FS2 is as low as 0.04 eV and the reaction is exothermic by 1.81 eV with respect to LH-IS2. The low barrier for formation of LH-FS3 and the small E_{ad} (-0.08 eV) of CO₂ indicate that the regeneration of PtBV as the available reaction center for subsequent CO oxidation is also a spontaneous process even at low temperatures.

We also investigated the possibility for CO oxidation to proceed through mechanisms other than the LH mechanism. As CO adsorption is more plausible than O₂ adsorption while coadsorption of 1 O₂ and 1 CO is more plausible than that of 2 CO, the adsorbed CO promoted O₂ activation mechanism may not hold for our case of PtBV.⁶⁸ The CO oxidation through the direct reaction of gaseous CO with adsorbed O₂ (ER1) proposed by Lin et al.⁴⁵ over Co atoms embedded in h-BN without, and proposed and observed by Li et al.³⁶ and Moser et al.²⁸ over Fe atoms embedded in graphene and Pt atoms dispersed on Al₂O₃ with (ER2) the formation of CO₃-like intermediate were both investigated (Figure S2, S3). We found that the barriers for formation and dissociation of the CO₃-like intermediate through ER2 mechanism are 0.92 and

1.31 eV, respectively, while that for the formation of LH-FS1 through ER1 mechanism without formation of CO_3 -like intermediate is 0.90 eV. The high reaction barriers (at least 0.90 eV for ER1 and ER2, as compared with 0.38 eV for the LH mechanism) and the low stability of the initial state (-1.95 eV for ER1 and ER2 *v.s.* -3.04 eV for LH) along ER mechanism suggest that LH mechanism is the primary mechanism for CO oxidation over PtBV. The thermodynamics profile of the MEP for CO oxidation over PtBV is schematically summarized in Figure 4.

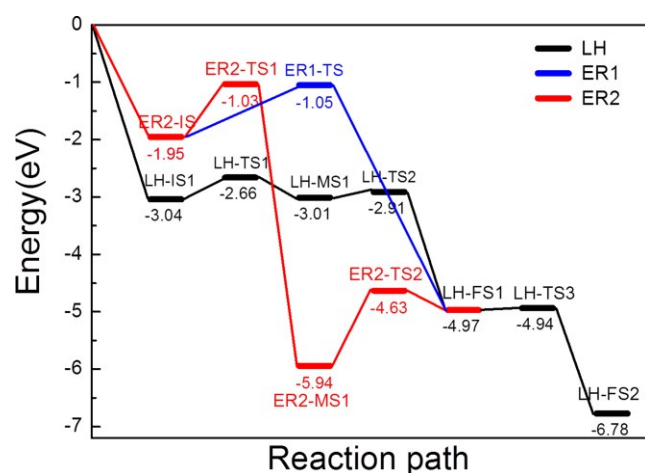


Figure 4. Schematic energy profile corresponding to local configurations shown in Figures 3, S2 and S3 along the MEP for CO oxidation over PtBV. All energies are given with respect to the reference energy, i.e., the sum of energies of the clean PtBV and gaseous CO and O_2 molecules.

In summary, the CO oxidation over PtBV may be characterized as a two-step process: The CO catalytic oxidation cycle is initiated through the LH mechanism, where the coadsorbed CO and O_2 (LH-IS1) react to form a peroxide like complex (LH-MS1), by the dissociation of which the a CO_2 molecule and an adsorbed O atom are formed (LH-FS1), and then the PtBV is regenerated to be available by the reaction of a gaseous CO with the adsorbed O atom (LH-IS2) to form another CO_2 (LH-FS2). We investigated the evolution of DOS of O_2 and CO states during the

reaction (Figure S4) and realized that the potential high catalytic performance of PtBV can be attributed to the compatibility of the states of PtBV and adsorbed intermediates, particularly among the upshifted Pt-d states originated from the Pt-N interaction, and the molecular states of CO and O₂, that facilitates the required charge transfer for the reaction to proceed. The enhancement of adsorption of CO, O₂ and CO₂ and the stability of intermediates that is nearly proportional to the upshift of Pt-d states also vigorously visualize this promotion effect resulting from the interfacial Pt-N interaction.⁶⁹

4. CONCLUSION

We investigated the electronic structure and predicted the catalytic performance in CO oxidation of Pt atoms stabilized by BVs on h-BN by first-principles based calculations. We showed that the Pt atoms use Pt-d and Pt-sp states to interact with the localized defect states on BV. This interaction is as strong as -4.40 eV, which not only prohibits the diffusion and aggregation of stabilized Pt atoms, but also shifts some Pt-d states to stand at the E_F. These upshifted dangling Pt-d states contribute to the enhanced reactivity and catalytic performance of PtBV. Facilitated by these upshifted Pt-d states that eventually satisfy the requirements for O₂ activation and subsequent reactions among coadsorbates, the CO oxidation over PtBV prefers to proceed through the LH mechanism and the barriers for the formation and dissociation of the O-O-C-O intermediate and the regeneration of PtBV for subsequent reaction are 0.38, 0.10 and 0.04 eV, respectively. These calculated barriers are among the lowest values ever reported suggesting the superiority of PtBV as catalyst for CO oxidation. These findings highlight the possibility to manipulate both the energy distribution of TM-d states and the easiness for donation of the TM-d electrons to adsorbates through defect engineering of the support material, and would be helpful for future design and implementation of high performance single-atom catalysts. These findings

also call for development of synthetic procedures that can fabricate defects over h-BN in a well-defined way for controlled deposition of transition metal atoms to achieve overwhelming catalytic performance.

ASSOCIATED CONTENT

Supporting Information. Comparison of DOS of PtBV and Pt(111), local configurations of the adsorbates on the PtBV at various states along the MEP via ER1 and ER2 mechanisms and evolution of CO and O₂ DOS along the MEP via LH mechanism. This material is available free of charge via the Internet at <http://XXX.XXX.XXX>.

AUTHOR INFORMATION

Corresponding Author

* Dr. Xin Liu, Tel: +86-411-84986343, Email: xliu@dlut.edu.cn.

Author Contributions

X. L. designed the research and wrote the manuscript. T. D. conceived the calculations and analyzed the results. T. D. is responsible for the calculation results. Y. H. and C.G. M. proofed the manuscript and polished the language. All authors have given approval to the final version of the manuscript.

ACKNOWLEDGMENT

This work was supported by NSFC (21373036, 21103015, 21271037 and 11174045), the Fundamental Research Funds for the Central Universities (DUT12LK14 and DUT14LK09), the Key Laboratory of Coastal Zone Environmental Processes YICCAS (201203), the Key Science and Technology International Co-operation Foundation of Hainan Province, China (KJHZ2014-

08) and the Special Academic Partner GCR Program from King Abdullah University of Science and Technology. Y. H would also thank Dalian University of Technology for the Seasky Professorship.

REFERENCES

1. A. Alavi, P. J. Hu, T. Deutsch, P. L. Silvestrelli and J. Hutter, *Phys. Rev. Lett.*, 1998, **80**, 3650-3653.
2. W. T. Yu, M. D. Porosoff and J. G. G. Chen, *Chem. Rev.*, 2012, **112**, 5780-5817.
3. R. Siburian, T. Kondo and J. Nakamura, *J. Phys. Chem. C*, 2013, **117**, 3635-3645.
4. S. Shan, V. Petkov, L. Yang, J. Luo, P. Joseph, D. Mayzel, B. Prasai, L. Wang, M. Engelhard and C.-J. Zhong, *J. Am. Chem. Soc.*, 2014, **136**, 7140-7151.
5. R. Toyoshima, M. Yoshida, Y. Monya, Y. Kousa, K. Suzuki, H. Abe, B. S. Mun, K. Mase, K. Amemiya and H. Kondoh, *J. Phys. Chem. C*, 2012, **116**, 18691-18697.
6. Z. P. Liu and P. Hu, *J. Chem. Phys.*, 2001, **115**, 4977-4980.
7. M. S. Chen, Y. Cal, Z. Yan, K. K. Gath, S. Axnanda and D. W. Goodman, *Surf. Sci.*, 2007, **601**, 5326-5331.
8. Z.-P. Liu, P. Hu and A. Alavi, *J. Am. Chem. Soc.*, 2002, **124**, 14770-14779.
9. M. L. Kimble, A. W. Castleman, R. Mitric, C. Burgel and V. Bonacic-Koutecky, *J. Am. Chem. Soc.*, 2004, **126**, 2526-2535.
10. R. Borup, J. Meyers, B. Pivovar, Y. S. Kim, R. Mukundan, N. Garland, D. Myers, M. Wilson, F. Garzon, D. Wood, P. Zelenay, K. More, K. Stroh, T. Zawodzinski, J. Boncella, J. E. McGrath, M. Inaba, K. Miyatake, M. Hori, K. Ota, Z. Ogumi, S. Miyata, A. Nishikata, Z. Siroma, Y. Uchimoto, K. Yasuda, K. I. Kimijima and N. Iwashita, *Chem. Rev.*, 2007, **107**, 3904-3951.
11. Q. Fu, W. X. Li, Y. X. Yao, H. Y. Liu, H. Y. Su, D. Ma, X. K. Gu, L. M. Chen, Z. Wang, H. Zhang, B. Wang and X. H. Bao, *Science*, 2010, **328**, 1141-1144.
12. B. T. Qiao, A. Q. Wang, X. F. Yang, L. F. Allard, Z. Jiang, Y. T. Cui, J. Y. Liu, J. Li and T. Zhang, *Nat. Chem.*, 2011, **3**, 634-641.
13. J. Lin, B. T. Qiao, J. Y. Liu, Y. Q. Huang, A. Q. Wang, L. Li, W. S. Zhang, L. F. Allard, X. D. Wang and T. Zhang, *Angew. Chem.-Int. Edit.*, 2012, **51**, 2920-2924.
14. B. Hammer and J. K. Norskov, in *Advances in Catalysis*, Academic Press Inc, San Diego, 2000, pp. 71-129.
15. I. N. Remediakis, N. Lopez and J. K. Norskov, *Angew. Chem.-Int. Edit.*, 2005, **44**, 1824-1826.
16. X. Liu, S. B. Zhang, X. C. Ma, J. F. Jia, Q. K. Xue, X. H. Bao and W. X. Li, *Appl. Phys. Lett.*, 2008, **93**, 093105.
17. L. Li, A. H. Larsen, N. A. Romero, V. A. Morozov, C. Glinsvad, F. Abild-Pedersen, J. Greeley, K. W. Jacobsen and J. K. Norskov, *J. Phys. Chem. Lett.*, 2013, **4**, 222-226.
18. X. F. Yang, A. Q. Wang, B. T. Qiao, J. Li, J. Y. Liu and T. Zhang, *Accounts Chem. Res.*, 2013, **46**, 1740-1748.
19. X. Liu, Y. Sui, C. Meng and Y. Han, *RSC Adv.*, 2014, **4**, 22230-22240.
20. X. Liu, C. Meng and Y. Han, *Nanoscale*, 2012, **4**, 2288-2295.
21. X. Liu, K. X. Yao, C. Meng and Y. Han, *Dalton Trans.*, 2012, **41**, 1289-1296.

22. X. Liu, L. Li, C. Meng and Y. Han, *J. Phys. Chem. C*, 2012, **116**, 2710–2719.
23. K. X. Yao, X. Liu, Z. Li, C. C. Li, H. C. Zeng and Y. Han, *ChemCatChem*, 2012, **4**, 1938-1942.
24. M. S. Chen and D. W. Goodman, *Chem. Soc. Rev.*, 2008, **37**, 1860-1870.
25. Y. X. Yao, X. Liu, Q. Fu, W. X. Li, D. L. Tan and X. H. Bao, *ChemPhysChem*, 2008, **9**, 975-979.
26. A. Uzun, V. Ortalan, Y. L. Hao, N. D. Browning and B. C. Gates, *ACS Nano*, 2009, **3**, 3691-3695.
27. A. Uzun, V. Ortalan, N. D. Browning and B. C. Gates, *J. Catal.*, 2010, **269**, 318-328.
28. M. Moses-DeBusk, M. Yoon, L. F. Allard, D. R. Mullins, Z. Wu, X. Yang, G. Veith, G. M. Stocks and C. K. Narula, *J. Am. Chem. Soc.*, 2013, **135**, 12634-12645.
29. A. A. Herzing, C. J. Kiely, A. F. Carley, P. Landon and G. J. Hutchings, *Science*, 2008, **321**, 1331-1335.
30. W. C. Ding, X. K. Gu, H. Y. Su and W. X. Li, *J. Phys. Chem. C*, 2014, **118**, 12216-12223.
31. P. P. Hu, Z. W. Huang, Z. Amghouz, M. Makkee, F. Xu, F. Kapteijn, A. Dikhtiarenko, Y. X. Chen, X. Gu and X. F. Tang, *Angew. Chem.-Int. Edit.*, 2014, **53**, 3418-3421.
32. S. Sun, G. Zhang, N. Gauquelin, N. Chen, J. Zhou, S. Yang, W. Chen, X. Meng, D. Geng, M. N. Banis, R. Li, S. Ye, S. Knights, G. A. Botton, T.-K. Sham and X. Sun, *Sci. Rep.*, 2013, **3**, 1775.
33. X. Liu, Y. Sui, T. Duan, C. Meng and Y. Han, *Phys. Chem. Chem. Phys.*, 2014, **16**, 23584-23593.
34. Y. H. Lu, M. Zhou, C. Zhang and Y. P. Feng, *J. Phys. Chem. C*, 2009, **113**, 20156-20160.
35. E. H. Song, Z. Wen and Q. Jiang, *J. Phys. Chem. C*, 2011, **115**, 3678-3683.
36. Y. Li, Z. Zhou, G. Yu, W. Chen and Z. Chen, *J. Phys. Chem. C*, 2010, **114**, 6250-6254.
37. Y. A. Tang, Z. X. Yang and X. Q. Dai, *Phys. Chem. Chem. Phys.*, 2012, **14**, 16566-16572.
38. M. Corso, W. Auwarter, M. Muntwiler, A. Tamai, T. Greber and J. Osterwalder, *Science*, 2004, **303**, 217-220.
39. A. Nag, K. Raidongia, K. Hembram, R. Datta, U. V. Waghmare and C. N. R. Rao, *ACS Nano*, 2010, **4**, 1539-1544.
40. S. Z. Butler, S. M. Hollen, L. Y. Cao, Y. Cui, J. A. Gupta, H. R. Gutierrez, T. F. Heinz, S. S. Hong, J. X. Huang, A. F. Ismach, E. Johnston-Halperin, M. Kuno, V. V. Plashnitsa, R. D. Robinson, R. S. Ruoff, S. Salahuddin, J. Shan, L. Shi, M. G. Spencer, M. Terrones, W. Windl and J. E. Goldberger, *ACS Nano*, 2013, **7**, 2898-2926.
41. A. Pakdel, Y. Bando and D. Golberg, *Chem. Soc. Rev.*, 2014, **43**, 934-959.
42. A. Zobelli, C. P. Ewels, A. Gloter, G. Seifert, O. Stephan, S. Csillag and C. Colliex, *Nano Lett.*, 2006, **6**, 1955-1960.
43. A. Zobelli, A. Gloter, C. P. Ewels, G. Seifert and C. Colliex, *Phys. Rev. B*, 2007, **75**, 245402.
44. C. H. Jin, F. Lin, K. Suenaga and S. Iijima, *Phys. Rev. Lett.*, 2009, **102**, 195505.
45. S. Lin, X. Ye, R. S. Johnson and H. Guo, *J. Phys. Chem. C*, 2013, **117**, 17319–17326.
46. P. Zhao, Y. Su, Y. Zhang, S.-J. Li and G. Chen, *Chem. Phys. Lett.*, 2011, **515**, 159-162.
47. C. J. Huang, X. X. Ye, C. Chen, S. Lin and D. Q. Xie, *Comput. Theor. Chem.*, 2013, **1011**, 5-10.
48. M. Gao, A. Lyalin and T. Taketsugu, *J. Chem. Phys.*, 2013, **138**, 034701.
49. X. Liu, T. Duan, Y. Sui, C. Meng and Y. Han, *RSC Adv.*, 2014, **4**, 38750-38760.
50. B. Delley, *J. Chem. Phys.*, 1990, **92**, 508-517.

51. B. Delley, *J. Chem. Phys.*, 2000, **113**, 7756-7764.
52. J. P. Perdew, K. Burke and M. Ernzerhof, *Phys. Rev. Lett.*, 1996, **77**, 3865-3868.
53. B. Delley, *Phys. Rev. B*, 2002, **66**, 155125.
54. X. Liu, C. G. Meng and C. H. Liu, *Phase Transit.*, 2006, **79**, 249-259.
55. X. Liu, C. G. Meng and C. H. Liu, *Acta Phys.-Chim. Sin.*, 2004, **20**, 280-284.
56. N. Govind, M. Petersen, G. Fitzgerald, D. King-Smith and J. Andzelm, *Comput. Mater. Sci.*, 2003, **28**, 250-258.
57. H. J. Monkhorst and J. D. Pack, *Phys. Rev. B*, 1976, **13**, 5188-5192.
58. F. L. Hirshfeld, *Theor. Chim. Acta*, 1977, **44**, 129-138.
59. M. Gajdos, A. Eichler and J. Hafner, *J. Phys.-Condes. Matter*, 2004, **16**, 1141-1164.
60. A. H. Castro Neto, F. Guinea, N. M. R. Peres, K. S. Novoselov and A. K. Geim, *Rev Mod Phys*, 2009, **81**, 109-162.
61. M. S. Chen and D. W. Goodman, *Science*, 2004, **306**, 252-255.
62. D. Matthey, J. G. Wang, S. Wendt, J. Matthiesen, R. Schaub, E. Laegsgaard, B. Hammer and F. Besenbacher, *Science*, 2007, **315**, 1692-1696.
63. J. H. Kwak, J. Z. Hu, D. Mei, C. W. Yi, D. H. Kim, C. H. F. Peden, L. F. Allard and J. Szanyi, *Science*, 2009, **325**, 1670-1673.
64. W. X. Li, C. Stampfl and M. Scheffler, *Phys. Rev. B*, 2002, **65**, 075407.
65. X. Liu, H. Guo and C. Meng, *J. Phys. Chem. C*, 2012, **116**, 21771-21779.
66. K. J. Laidler, *Pure Appl. Chem.*, 1996, **68**, 149-192.
67. C. Liu, Y. Tan, S. Lin, H. Li, X. Wu, L. Li, Y. Pei and X. C. Zeng, *J. Am. Chem. Soc.*, 2013, **135**, 2583-2595.
68. K. K. Mao, L. Li, W. H. Zhang, Y. Pei, X. C. Zeng, X. J. Wu and J. L. Yang, *Sci Rep*, 2014, **4**, 5441.
69. W. An, Y. Pei and X. C. Zeng, *Nano Lett.*, 2008, **8**, 195-202.

